CHALMERS
UNIVERSITY OF TECHNOLOGY

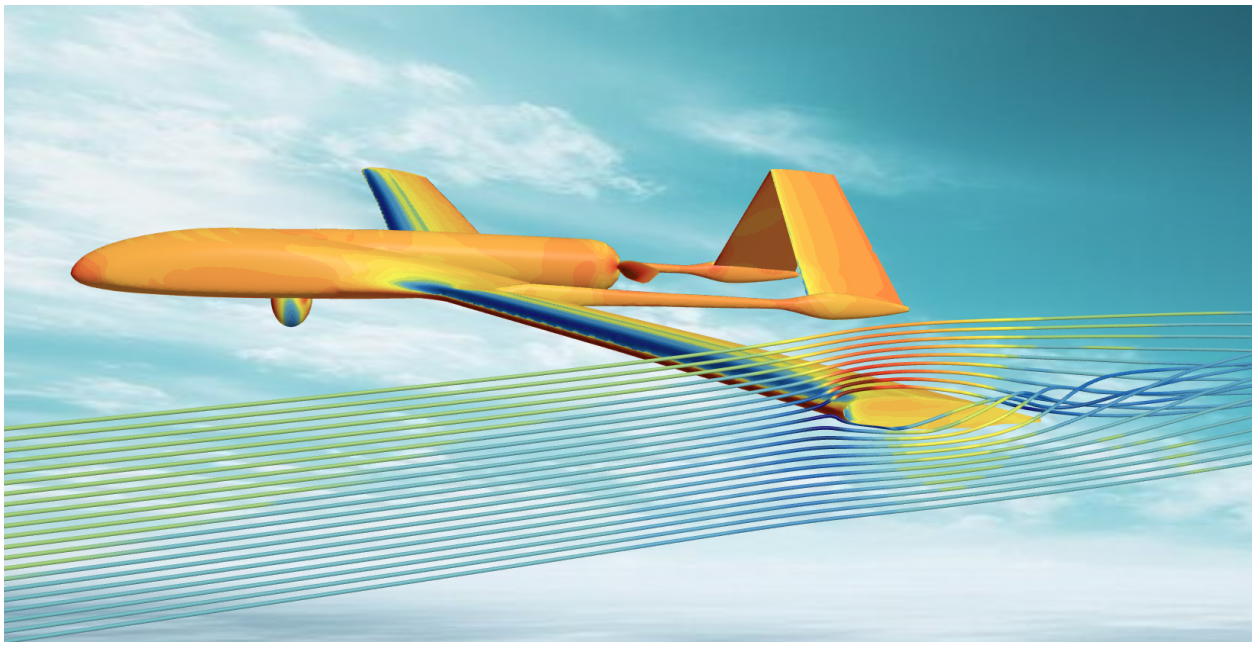

Numerical investigation of long-span wing drone aeroelastic behavior using Lattice Boltzmann method

Master's thesis in Mechanics and Maritime Sciences

ADAM KAŠIČKA

DEPARTMENT OF MECHANICS AND MARITIME SCIENCES

CHALMERS UNIVERSITY OF TECHNOLOGY
Gothenburg, Sweden 2025
www.chalmers.se

Master's thesis 2025

Numerical investigation of long-span wing drone aeroelastic behavior using Lattice Boltzmann method

Adam Kašička

CHALMERS
UNIVERSITY OF TECHNOLOGY

Department of Mechanics and Maritime Sciences
Division of Fluid Dynamics
Chalmers University of Technology
Gothenburg, Sweden 2025

Numerical investigation of long-span wing drone aeroelastic behavior using Lattice Boltzmann method
ADAM KAŠIČKA

Email: adamkasicka2@gmail.com

Supervisor: Huadong Yao, Mechanics and Maritime Sciences
Examiner: Huadong Yao, Mechanics and Maritime Sciences

Master's Thesis 2025
Department of Mechanics and Maritime Sciences
Division of Fluid Dynamics
Chalmers University of Technology
SE-412 96 Gothenburg
Telephone +46 31 772 1000

Cover: Wing tip streamlines visualization showing the air velocity with the skin friction on the drone geometry conducted in Star CCM+.

Printed by Chalmers Reproservice
Gothenburg, Sweden 2025

Numerical investigation of long-span wing drone aeroelastic behavior using Lattice Boltzmann method
ADAM KAŠIČKA
Department of Mechanics and Maritime Sciences
Chalmers University of Technology

Abstract

This work is focused on dealing with the fluid structure interaction (FSI), FSI is one of the great engineering challenges, due to its complexity that occurs when the fluid is acting on the object in the way that the object from the fluid flow forces is deforming and changing back the fluid flow behavior around the object. This type of interaction occurs in many different engineering challenges and is one of the key reasons why many people are drawn to the engineering field.

The aim of this project is to conduct a fluid structure interaction analysis on the unmanned aerial vehicle Bayraktar TB2, and its impact on the performance from the deformation caused by the lift forces. Nowadays, there is a demand for drones as they can operate long distances with high accuracy and endurance, which means that for more demanding operations, these unmanned aerial vehicles are growing in size and speed [13]. As some of these drones have long-span wings, this means that they underlie a significant lift force in order to compensate for the weight, therefore, we will investigate how these long-span wings behave in cruise condition during the real mission.

The geometry has been created with respect to the existing drone geometry, Bayraktar TB2. For the development of 3D geometry, we used OpenVSP, a software used to create aerospace geometries. The fluid model has been carried out and conducted with respect to the actual mission. The domain of numerical investigation of the fluid flow field has been carried out in Palabos, an open-source CFD software that uses the Lattice Boltzmann method. It is used for the advantages of reduced computational time and simple parallelization. CFD simulation is used to define the forces acting on the geometry and also to evaluate the performance of the drone. In order to model the deformation of the long-span wings, we will use the forces from the CFD simulation as boundary conditions, the main focus will be on the lift, as this force will be significantly higher than drag. For structural simulation, we will use the Ansys static structural solver to investigate and model the wing deformation. After the structural simulation, we will export the deformed geometry to use it in the CFD simulation to investigate changes in performance and the flow field.

The differences in performance have been analyzed, and the results have been compared to judge whether or not the deformation significantly reduces the performance of the long-span wing drone in the cruise conditions.

Keywords: FSI, drone, Lattice Boltzmann method, CFD, FEM, aerodynamics, wing deformation, lift force, drag force.

Acknowledgements

In the first place, I would like to thank my professor and supervisor, Huadong Yao, for his patience, valuable insights, and priceless pieces of advice throughout the making of this master's thesis. I also want to thank Chalmers University of Technology and professors from all my courses for the education and knowledge they provided me with, which I will use in my professional life.

Adam Kašička, Gothenburg, June 2025

List of Acronyms

Below is the list of acronyms that have been used throughout this thesis listed in alphabetical order:

CFD	Computational Fluid Dynamics
LBM	Lattice Boltzman Method
FVM	Finite Volume Method
AOA	Angle Of Attack
FEM	Finite element method
FSI	Fluid structure interaction
UAV	Unmanned aerial vehicle

Nomenclature

Below is the nomenclature of indices, sets, parameters, and variables that have been used throughout this thesis.

Latin Symbols	
A	Frontal Area (m^2)
C_l	Coefficient of lift
C_d	Coefficient of drag
E	Tensile modulus
f	particle distribution function ()
F	Force (N)
F_l	Lift force
F_d	Drag force
g	Acceleration due to gravity (m/s^2)
k	Stiffness constant
L	Characteristic length (m)
Ma	Mach number
m	Mass (kg)
P	Pressure (Pa)
R	Ideal gas constant
Re	Reynolds number
T	Temperature (K)
t	Time (s)
$u(LB)$	Lattice Boltzmann velocity
cs	speed of sound (LB)
V	Velocity
v	viscosity
x, y, z	Cartesian coordinates (m)
Greek Symbols	
μ	Dynamic viscosity (Pa·s)
ρ	Density (kg/m^3)
σ	Tensile stress (Pa)
τ	relaxation time
ϕ	Relative humidity (dimensionless)
ω	Angular velocity (rad/s)
ξ	microscopic velocity (rad/s)
Ω	collision operator
ε	strain

$\mathcal{H}$	entropy of thermodynamics

Contents

List of Figures

List of Tables

1
Introduction

This Master's thesis is focused on making and investigating a long-span wing drone based on Bayraktar TB2, its aeroelasticity performance is investigated using the Lattice Boltzmann method in open source code Palabos. The fluid structure interaction, or FSI, is a phenomenon that combines multiple physics problems, which usually consist of systems where the object is being deformed due to it being subject to the force from the fluid flow. This phenomenon can also act in reverse, which means that the deformation of the mentioned object can change the fluid flow behaviour around the object, the force on the object, and the investigated object's aerodynamic performance. This kind of interaction can occur in various engineering and natural systems. The FSI investigation plays a very important role in designing and analyzing various engineering systems during the development phase of the new systems or optimizing and improving an existing one. It also helps to identify flaws and faults before the component or system is manufactured, and therefore, it can be very useful for saving resources before testing the real manufactured system or component [15]. FSI investigations have a wide range of applications; for instance, they can be applied to investigate the flutter on aircraft wings or to better understand the mechanisms of microorganisms.

FSI simulations are becoming more and more important in the field of numerical investigations and analyses due to the fact that it can resolve the real life situations better and more accuratelly which means that if the correlation between computational simulations and for example wind tunnel or real life testing is precise than we can save manufacturing time and resources due to the fact that most of the problems, that would occur in wind tunnel or real life testing, can be solved even before manufacturing of the systems or components.

1.1 Background

In the recent years the technology of the observation and reconnaissance with the use of the unmanned aerial vehicles (UAV) is accelerating and nowadays it is widely used to observe strategic locations without spending too much resources in terms of full scale plane with pilot and crew on board, instead now there is huge demand for having the ability to observe the locations that can be very far away with a controlled drone with high resolution Lidar or camera [13]. These large drones usually consist of a long-span wing, which provides great aerodynamic efficiency but comes at the cost of significant structural stress. These long-span wing drones

are usually heavy, and they can weigh almost up to a small ultralight plane, so the lift provided in order to keep them flying has to be proportional to their weight. This means that the long-span wing drone can be subject to huge moments and, therefore, a risk of significant deformation, which can then have an effect on the aerodynamic performance of the drone. This fluid structure interaction needs to be investigated in order to understand how the mentioned performance changes with the deformation changes. These drones are usually propelled by small turboprop engines, which are also going to be included in the CFD simulations and are essential for the aerodynamic performance investigation. In order to make a large number of full-scale transient CFD simulations, we are going to use Lattice Boltzmann method-based CFD software, which has become more and more popular in recent years because of its parallelization and speed compared to the traditional Finite Volume method [10][17].

1.2 Purpose

It is known that the aircraft wings are deflecting during flight conditions and aircraft manufacturers are taking this into account but until now there weren't that many large span wing drones flying, and because they are progressively getting bigger and faster we also need to investigate this behavior in order to understand what impact it has on the drones performance during the cruise conditions, and for this investigation we are going to use the new method of CFD simulation which is rapidly growing in demand in recent years, because of its efficiency, speed and accuracy compared to the more traditional Finite Volume Method (FVM) of numerical investigation. Also, to get the view of how the widely used existing drone performs aerodynamically, and to try to improve its performance with LBM CFD simulations [17].

1.3 Objectives

With the mentioned purposes in mind, we will now mention the goals we aim to achieve in this project:

- To develop a geometry of the existing drone based on the found pieces of information and parameters
- To develop a numerical investigation method for the large span wing drone using the Lattice Boltzmann method, using a coupling FSI analysis
- To investigate the structural behavior of the drone under the forces from the fluid flow and the impact of the structural deformation on the aerodynamic performance
- To evaluate and analyse the results and draw conclusions based on them

1.4 Assumptions and simplifications

The points below are the considerations made in order to reduce computational resources, time, and to get reasonable outcomes from this project.

- The geometry used has been made to look as close as possible to the existing drone, but it is certainly not 1:1, so the differences from reality will also have an impact on the performance and the deformation.
- The material used in structural simulation is not the only one that the drone uses, but because it is hard to get detailed information for this type of drone, we will assume it is mostly carbon fiber.
- The aerodynamic simulation will be conducted at the cruise condition, so the loads can increase, for example, during takeoff or climb, but for this project, we chose to investigate the performance during cruise, where we think the aircraft spends most of the operational time.
- The domain and mesh resolution in the CFD simulations were set according to the computational and memory limitations.
- The lift force from the CFD simulations will be assumed to be sufficient to accommodate the weight of the drone because of the mentioned possibility of performance variation.

2

Theory

As mentioned in the introduction part, this project will focus on FSI investigation, which combines CFD and FEM simulations, and therefore it is important to grasp the common priciples and equations used in both of these simulations to understand the different methods of FSI and results of this project. Below, we will describe different approaches to FSI.

2.1 Coupling approaches

In the following sections, we will discuss different approaches for coupling the fluid flow simulations with the structural simulations. As we will use both of them in this project, it is important to understand how the methodology of the coupling works.

2.1.1 Monolithic approach

In the monolithic approach, both of the problems, fluid and structural, are treated in the same mathematical framework to conduct a single system of equations for the whole problem. This problem is then solved at once by a merged algorithm. In this method, the interaction between the fluid and the structure will be treated simultaneously at the interface [11].

Figure 2.1: Monolithic approach

2.1.2 Partitioned approach

In this type of approach to the FSI problem, both subdomains are solved separately, they can be solved in two different software or solvers. This essentially means that the conservation of properties of continua is lost [11].

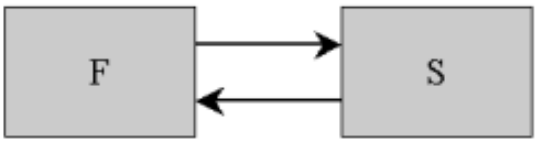

Figure 2.2: Partitioned approach

2.1.3 Single solution approach

In the single solution approach, the fluid and solid subproblems are solved simultaneously for each time step in a single solution domain. One set of equations describes both of the subdomains, and the solution domain also includes the interface, which makes the coupling itself inherently implicit [11].

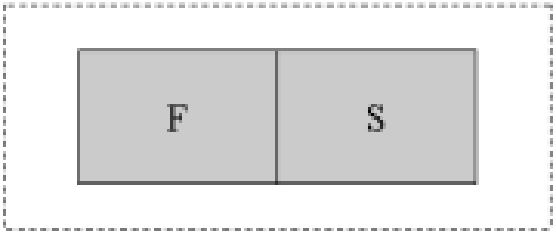

Figure 2.3: Single solution approach

2.1.4 One-way coupling

We can consider the coupling as one-way if the forces from the fluid flow influence the investigated structure in a way that the deformation or the reaction of the solid is negligible. This theory also holds the other way around.

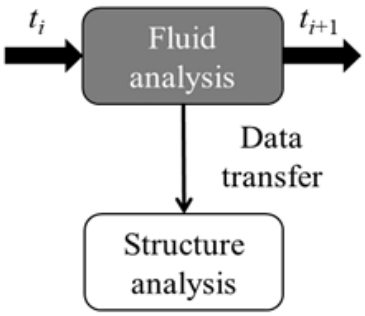

Figure 2.4: One-way coupling

On the figure above we can see the workflow of the one-way coupling. First the fluid analysis is performed, and then the forces due to the fluid are transferred to the solid solver to perform structural simulation, and this is repeated until it reaches the final time value.

2.1.5 Two-way coupling

This type of coupling happens when there is a significant force from the fluid flow induced on the investigated structure, and this results in a deformation that can no longer be neglected. We have to go back to the fluid analysis to investigate the behavior of the deformed structure.

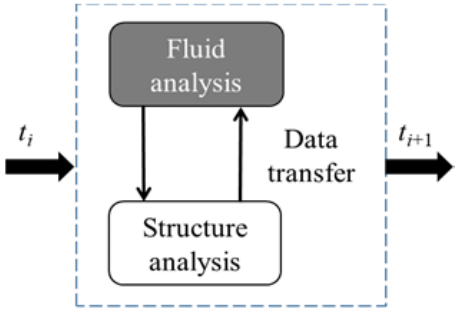

Figure 2.5: Two-way coupling

The working principle of the two-way coupling method is similar to the one-way, in the sense that the forces exerted on the structure from the fluid are interpolated to the structural simulation, but because now the deformation is significant we export the deformed mesh back to the fluid analysis software to update the geometry of the fluid domain [15].

2.2 CFD

In this part, we will discuss the Lattice Boltzmann method used in the chosen software Palabos to numerically investigate the aerodynamic performance of the long-span wing drone geometry. As mentioned earlier, this method of fluid flow simulation is different from the conventional Finite Volume Method (FVM) used in the industry, therefore, the main differences and workflow of this method are explained below.

2.2.1 Lattice Boltzmann Method

When we are talking about the Lattice Boltzmann Method (LBM) compared to the Finite Volume Method (FVM), it is important to start by introducing the macroscopic scale and the microscopic scale. In the FVM, people tend to look at the macroscopic scale, which means that they don't look at the individual particles but more at the flow field as a whole. If ocean waves are observed, it is clearly visible in which direction they are traveling. In this way, it is possible to determine the traveling direction of the mass of water, but on the microscopic scale If the individual particles would be observed, then it would be impossible to determine where the mass that these particles are part of, is headed to, because the particles would seem to behave in a chaotic way, and that each individual particle has a different direction from the one next to it. If we were to investigate, for example, an empty room where

there is seemingly no velocity of the air, on the macroscopic scale, we would think there is zero velocity of the air, but on the microscopic scale, we would see that the particles are moving and colliding nonstop. If we sum the velocity vectors of each particle, we would get 0, but the magnitude isn't going to be zero, which explains this behavior on the macro and microscopic scale [2].

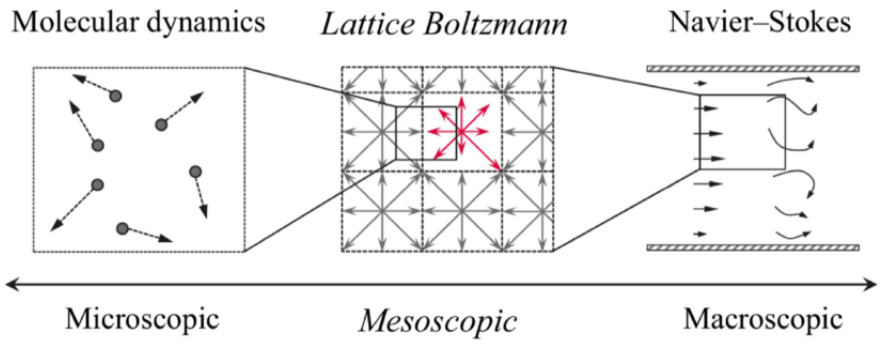

Figure 2.6: Relation between microscopic, mesoscopic, and macroscopic scale

In the LBM as we can see on the Figure 2.1 we are on the mesoscopic scale which means that we are not investigating the individual particles but we are doing a statistical analysis of multiple particles, and in that way we know, how to predict the behavior of the groups of these particles in the investigated situations. There is a common misconception that LBM is assigned to a certain scale, however, this is not true because we can use LBM to numerically investigate, for example, blood flow in the blood vessel or airflow around full-scale aircraft, so the LBM has a very large field of application.

2.2.2 Kinetic theory

When we talk about the Lattice Boltzmann Method, we have to first start by introducing its cornerstone, the Kinetic theory. Kinetic theory describes the behavior of the fluid on the level that, as we already know, lies between the micro and macroscopic scales. On the microscopic scale, we are looking at each individual particle and its behavior, while on the macroscopic scale, we can describe the fluid using more tangible quantities such as density, pressure, velocity, and temperature, as is done using FVM. In the mesoscopic working scale of kinetic theory, we are describing the distribution of the particles, this quantity evolves on the timescales around the mean collision time t_{mfp}. Kinetic theory can be used in principle for any gases, but it best describes dilute gases, dilute monoatomic gases to be exact. We can assume there that the molecules spend very little time colliding ($t_c \ll t_{mfp}$), where t_c is the colliding time, and we can assume that colisions happen instantaneously, therefore $t_c \to 0$. With this in mind, we can go further and assume that the collisions happen only one particle on another particle almost every time and that there are close to no collisions of 3 or more particles. However, this assumption does not hold well for dense gases, where particles spend more time colliding because they are closer together, and it is also problematic for liquids, where the molecules hold together by intermolecular forces. We know that collisions conserve the quantities of mass,

momentum, and, in our monatomic case, translational energy. These conservation constraints can be represented as moments of the collision operator, which we will introduce later, but before that, we will describe the main variable of this theory [2].

2.2.2.1 Distribution function

The main variable when we talk about kinetic theory is the particle distribution function $f(x,\xi,t)$. When you look at it, you might think that it is a generalization of the density with the microscopic velocity ξ included. The difference is that the $\rho(x,t)$ is representing the density of mass in the general physical field and the particle distribution $f(x,\xi,t)$ function is on top of that representing the mass in the velocity field as well [2]. Because of this, the units of the particle distribution function are as follows:

$$[f] = \mathrm{kg} \times \frac{1}{\mathrm{m}^3} \times \frac{1}{(\mathrm{m/s})^3} = \frac{\mathrm{kg\ s}^3}{\mathrm{m}^6}. \tag{2.1}$$

We can say that this function is describing the particle's density at time t, at position x, and with its microscopic velocity ξ.

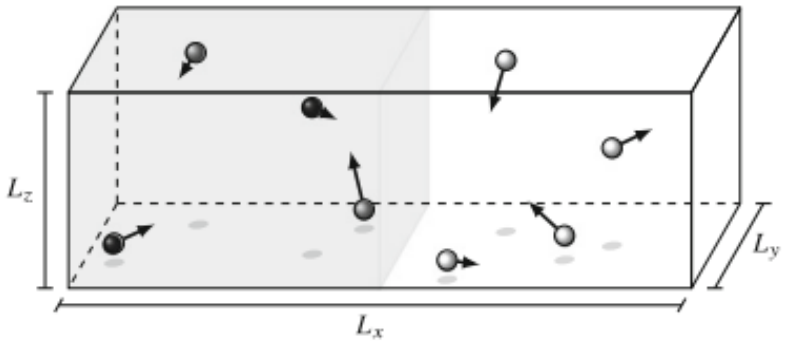

Figure 2.7: Particles that are black, and are in the left side of the box, have the microscopic velocity ξ_x>0 and therefore we can say that they are moving to the right

We can connect the macroscopic variables to the distribution function by its moments. We can get these moments by integrating the function. For example, we can get the macroscopic density as:

$$\rho(x,t) = \int f(x,\xi,t)\mathrm{d}^3\xi \tag{2.2}$$

If we integrate over the velocity space like this, we include the particles with all velocities that are at position x at time t. Another important parameter is the already mentioned velocity in the macroscopic space, which we can obtain from:

$$u(x,t) = \xi(x,t) - v(x,t) \tag{2.3}$$

The relative velocity v is how we can see the difference between the particle velocity and the local mean velocity. The relative velocity is part of the internal energy

density equation, which, as a moment, has the form of:

$$\rho(x,t)e(x,t) = 1/2 \int |v^2| f(x,\xi,t) \mathrm{d}^3\xi \tag{2.4}$$

Subsequently there are two ways to find the pressure, we can find it also as a moment of the distribution function, when we think about the fact that the particles are giving away their momentum during the process of bouncing off the surface, and as their velocity increases, then so does the momentum that they give away during the process of bouncing, and also with the increased velocity, bigger number of particles will have an ability to bounce off.

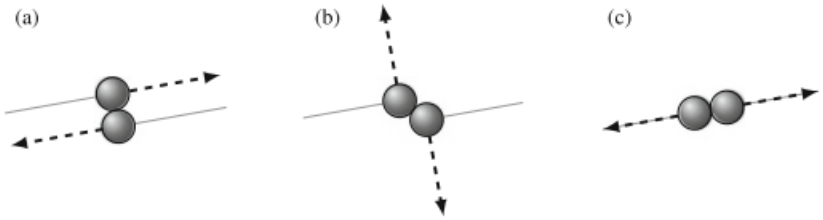

Figure 2.8: Collisions that can happen between two particles. (a) Grazing collision. (b) Angled collision. (c) Head-on collision

The second way of finding the pressure expression is by using the equipartition theorem, which gives the RT/2 specific internal energy for the typical degrees of freedom, which are rotation, molecular translation, and vibration, but for monoatomic gases, which we assume we are working with, there is no rotation or vibration. So the only degree of freedom left is molecular translation, and using the ideal gas law for monoatomic gas gets us:

$$\rho e = 3/2 \rho RT = 3/2 p \tag{2.5}$$

We can use almost the same moment as for the internal energy to find pressure as well as temperature[2].

$$p = \rho RT = 2/3 \rho e = 1/3 \int |v^2| f(x,\xi,t) \mathrm{d}^3\xi \tag{2.6}$$

2.2.3 Boltzmann equation

Now that we have a basic understanding of how the LBM works, we can dive into the question of why it works like that. For that, let me introduce the Boltzmann equation upon which the LBM is built, but first, we have to start off with the basics. In the FVM, we have the density ρ with pressure p, and 3 velocity vectors (ux, uy, uz). In the LBM, as we already learned, there is a distribution function $f(x,\xi,t)$, which tells us on which position x the particle is at time t and with what corresponding molecular velocity ξ [2].

$$\frac{df}{dt} = (\frac{\partial f}{\partial t})\frac{dt}{dt} + (\frac{\partial f}{\partial x_\beta})\frac{x_\beta}{dt} + (\frac{\partial f}{\partial \xi_\beta})\frac{d\xi_\beta}{dt}. \tag{2.7}$$

$$\frac{\partial f}{\partial t} + \xi_\beta \frac{\partial f}{\partial x_\beta} + \frac{F_\beta}{\rho} \frac{\partial f}{\partial \xi_\beta} = \Omega(f). \tag{2.8}$$

If we look closely at the right-hand side, we can see the Ω, which is a commonly noted total differential. On the left-hand side, we see the distribution function advected with velocity ξ, and the last term represents the forces that are influencing this velocity. The Ω is, in simple terms, considered as a source term, and it is known as a redistributor of f due to collisions, and that is why it is also called the collision operator [2].

2.2.4 Lattice Boltzmann equation

The fundamental quantity in the Lattice Boltzmann Method (LBM) is the discrete velocity distribution function, denoted as (x,t), which is often referred to as the particle population. This function, similar to the one introduced in Section 1.3, describes the density of particles moving with a specific discrete velocity at a given location x and time t. From this distribution, key macroscopic quantities such as the mass density and momentum density at point (x,t) can be derived through moment summations over the distribution functions:

$$\rho(x,t) = \sum_i f_i(x,t), \quad \rho u(x,t) = \sum_i c_i f_i(x,t). \tag{2.9}$$

Unlike the continuous particle distribution function f, the discrete function f_i uses only discrete variables. The subscript i is indicating a specific velocity c_i from a finite set of c_i velocities. The values of f_i are defined on a square lattice with spatial spacing Δx, and only at discrete time steps separated by Δt. These spacings, Δx and Δt, define the resolution of the simulation. While they can be expressed in units like SI or Imperial, most LBM applications use lattice units, where Δx=1, and Δt=1. Converting between lattice and physical units is straightforward, much like switching between unit systems. Alternatively, by matching key dimensionless quantities such as the Reynolds number or Mach number, which we will discuss later, we can simulate the same fluid flow behavior across different unit systems [2].

2.2.4.1 Collision operator

We already have the knowledge that during the particle collisions, quantities such as mass, momentum, and, as we mentioned earlier, translational energy, as well in the monoatomic case, are conserved. We can express these conservation laws as moment conditions in a very similar way to how we expressed the macroscopic density or internal energy density earlier, and we can apply them to the collision operator:

$$\Omega(f) = \frac{df}{dt} \tag{2.10}$$

The original collision operator invented by Boltzmann has a form of double integral over a velocity space, to consider every outcome of two-particle collision possible, which is very complicated and requires a lot of calculations. Fortunately, the general collision operators that we will encounter in the LBM software, such as the one we will use for this project, are based on the simpler BGK collision operator [2].

2.2.4.2 BGK collision operator

The CFD software Palabos that is used in this project, where the simulation is conducted to investigate the fluid flow, uses the BGK collision operator, which is most suitable for the gas simulation, which is also our case. The Bhatnagar-Gross-Krook or BGK collision operator has a form of:

$$\Omega_i = -\frac{f_i - f_i^{\mathrm{eq}}}{\tau}. \tag{2.11}$$

This operator directly captures the relaxation of the distribution function towards the equilibrium distribution. The parameter that determines the speed at which the equilibrium is reached is called the relaxation time, and it is denoted as τ [2].

2.2.5 Boltzmann's $\mathcal{H}$-Theorem

We can relate entropy's thermodynamic property directly to the distribution function f. Density of that entropy has a notation ρs and units: $[\rho s]{=}J/kgm^3$. It was Ludwig Boltzmann who showed that this quantity has the form of:

$$\mathcal{H} = \int f \ln f \, \mathrm{d}^3\xi \tag{2.12}$$

If we look at the eq(2.7), it can be observed that if we multiply that equation by $(1 + \ln f)$, with a few clever mathematical operations, it can be found that at the end, we get:

$$\frac{\partial}{\partial t}\int f \ln f d^3\xi + \frac{\partial}{\partial x_\alpha}\int \xi_\alpha f \ln f d^3\xi = \int \ln f \Omega(f) \, \mathrm{d}^3\xi \tag{2.13}$$

This represents the balance equation, and we can also find it as a moment, as we did earlier for the macroscopic density, for example. The second integral on the left-hand side represents the flux of the $\mathcal{H}$ quantity. We can divide it into two components: advective and diffusive. As we are interested in the previously described BGK collision operator, which can be in this theory found non-positive, which means that $\mathcal{H}$ is not conserved and that it only decreases, leading to the equilibrium state. The theorem basically states that the collisions are pushing the distribution function towards the equilibrium state. We can also show that $\mathcal{H}$ is proportional to the entropy density

$$\rho s = -R\mathcal{H} \tag{2.14}$$

, and that entropy only increases until the equilibrium state is reached, which is also when we reach the maximum entropy value [2].

2.3 Aerodynamics

In this section, I would like to touch upon the basic aerodynamic principles that are important in order to understand how the performance from the numerical investigation is evaluated, and also to help you understand the results of the calculations mentioned in the previous sections.

2.3.1 Lift and Drag

When we talk about pressure and velocity, we have to understand how it affects the investigated structure, in this case, an aircraft. Aircraft wings generate lift by making the pressure difference between the top of the wing and the bottom of the wing. On top, the wing generates lower pressure by accelerating the air or making higher velocity of the air. Contrary, at the bottom of the wing, there is either ambient or slightly higher pressure, which makes the difference in pressure. In very simplistic words, the higher-pressure region of air tends to go to the lower-pressure region, resulting in the force that we call a lift force. In this project, the main focus will be on investigating the FSI of wings and the impact of the deformation due to the lift force on the performance. The expression for lift force is:

$$F_l = 1/2\rho V^2 A C_l \tag{2.15}$$

On the left-hand side, we have the lift force, and on the right-hand side, we have air density ρ, air velocity squared, multiplied by frontal area A, and the coefficient of lift, which is essentially how good the shape is aerodynamically. Subsequently, the drag force is the same as the lift force, but it is calculated on the axis that goes along the object, while the lift force is perpendicular to the drag force. The expression for the drag force looks very similar to the lift force:

$$F_d = 1/2\rho V^2 A C_d \tag{2.16}$$

Here, we replace the lift coefficient with the drag coefficient, and the result is the drag force.

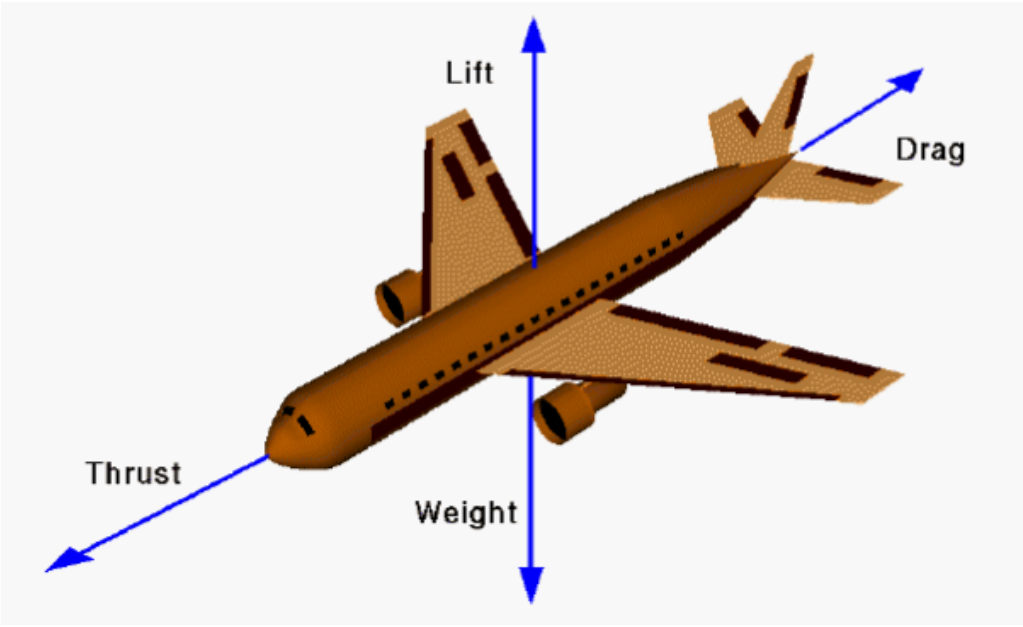

Figure 2.9: Forces acting on an aircraft

[1]The non-dimensional quantities such as Mach number and Reynolds number will be mentioned in the method section, where we also discuss the importance when

comparing these quantities to the real mission and how we convert the LB units to get the desired Reynolds and Mach numbers. In aircraft aerodynamics, probably the most important aspect for the overall aerodynamic performance of an aircraft is the airfoil. Airfoils are basically cross-sections of the wing, and they dictate the mentioned performance of the wing, but also the whole aircraft [10].

2.3.2 Airfoils

There are different types of airfoils for various applications. For example, on the aircraft, we could observe different airfoils on the main wing and empennage or tail wings. The main wing of the aircraft will be using a cambered airfoil to generate lift, but on the empennage, we will most likely see a symmetrical airfoil because the tail wing serves a purpose to stabilize the aircraft and give the pilot additional maneuverability. The purpose of the airfoil is, in most cases, to generate lift or downforce (negative lift). Their main function is to provide a reduced resistance to incoming air flow. They do this by guiding the air over the leading edge and, in turn, reducing the turbulent wake behind the airfoil. The degree of its performance is characterized by several parameters, such as chord length, angle of attack, airfoil shape in general, camber, etc.

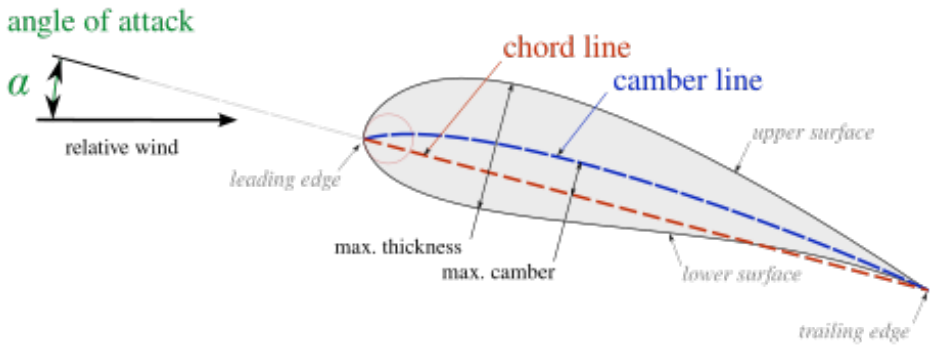

Figure 2.10: Airfoil

Airfoils play a crucial role during the design phase of any aircraft or anything that intends to generate lift or downforce using the air. Most of the companies usually are keeping secret what airfoil they are using or have developed. Chapter 3 will explain the method of obtaining the airfoil used for our drone [16].

2.4 Finite Element Method and structural model

In this project, we will evaluate both the flow field behavior around the object, which we covered in the previous chapters, and the structural response to the forces from the fluid. The following subsections will cover the basic theory needed in order to understand the numerical method, and results that we obtain from the structural investigation and the Finite Element method (FEM).

2.4.1 Static analysis

Because we are investigating the FSI in the cruising condition, we can assume that the lift force is uniformly distributed along the wings. There are two different types of loads acting on a structure. The first type is static load which does not vary with time and gives enough time for a structure to respond, whereas the second one, called dynamic load, changes with time quickly compared to the static loads. Impulse load is a kind of dynamic load, acts on the system or structure with a larger magnitude within a short interval of time. We will be investigating the static load because we assume, that this type of load will also occur during the real mission. As I already mentioned, the lift force is assumed to be uniformly distributed, and then we can think about the wings as a beam that is supported by the fuselage.

2.4.2 Beam theory

These beams are then exposed to the bending moments. Bending occurs when the transverse load is acting on the beam, which results in a change of its curvature. The deflection is a phenomenon during which we can observe a displacement of the beam points in the physical space. Beam bending can occur in the case of an external bending moment or a transverse force. Pure bending occurs in the first case, when only a normal stress is created in the beam cross-section, caused by the stretching of the upper fibers and the compression of the lower fibers of the beam in the cross-section.

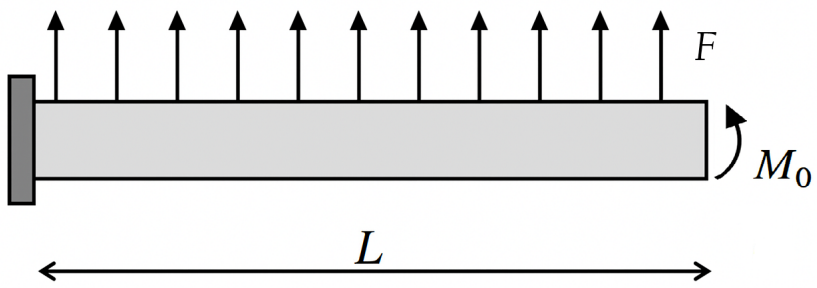

Figure 2.11: Beam with corresponding length L that is subject to uniquely spread force F and bending moment M_0

Under these conditions, the object returns to its original shape and size when the load is released. The elastic behavior of solids according to Hooke's law can be

explained by the fact that small displacements of molecules, atoms, or ions of solids from their normal positions are also proportional to the force that causes the displacement. A deforming force can be applied to a solid such that it will stretch, compress, bend, or twist it. Thus, the component will exhibit elastic behavior according to Hooke's law, because of the small increase in its length when stretched, due to the applied force is doubled whenever the force is also doubled Mathematically, Hooke's law can be expressed using the equation as

$$F = kx \tag{2.17}$$

where F is the applied force, which is equal to the elongation or change in the length of the part x, multiplied by the constant k. The value of the constant k depends not only on the type of material from which the part is made, but also on the dimensions and shape of the part itself must be taken into account [7].

2.4.3 Nonlinear deformation

Because this project will be conducted around the drone structure that is manufactured primarily as a carbon fibre monocoque, we can assume the non-linear behavior of the wings. With composite materials such as carbon fibre, it is difficult to predict the exact behavior. From the Hooke's law, we can derive the equation to calculate the tensile stress on the investigated structure. This equation has the form:

$$\sigma = E \cdot \varepsilon \tag{2.18}$$

We can see that E represents tensile modulus of elasticity of the material, σ tensile stress and ε strain, which for materials like structural steel or aluminium is well known, but for carbon fibre it differes with layup and we would have to conduct a test in order to find the exact material properties. However the Ansys has its own library with materials like carbon fibre, which we will use for our project [7][9].

2.4.4 Materials and stiffness

The main material that the structure of the drone is made of is carbon fibre. To be precise, it is carbon fibre monocoque, which means that there are very few parts made alone and the entire structure is made as one which improves the stiffness and structural behavior. Which means that the structure should withstand even what would otherwise be considered significant loads. Carbon fibre, compared to structural steel, which is also widely used in aviation, has a better stiffness-to-weight ratio, therefore, the structures built from carbon fibre composites are lightweight yet keep very good structural stiffness. The usual structure of a carbon fibre component is displayed in the figure [6][18][19].

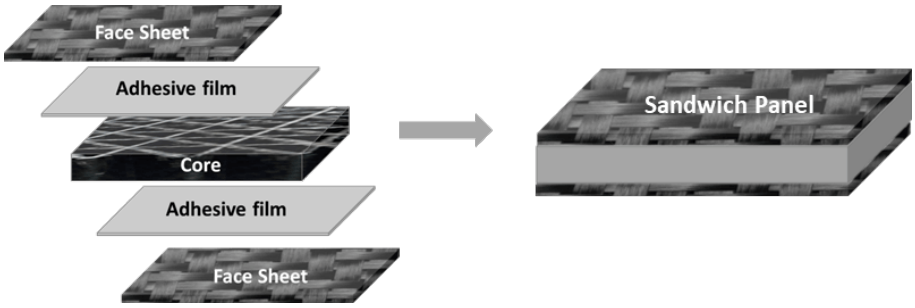

Figure 2.12: Carbon fibre sandwich

3

Methods

In this chapter, we will discuss the methodology that was followed in order to achieve an accurate investigation of the long-span wing drone aeroelasticity. We will cover the geometry development in OpenVSP, together with the Lattice Boltzmann CFD simulation performed in Palabos, and the structural part of this FSI investigation will be performed in the Ansys static structural solver to evaluate the structural loads and deformation of the structure. The boundary conditions for this case were established to investigate and replicate the cruise conditions that occur during the real mission, therefore, the loads might get significantly higher in the off-design conditions, but this was not what we were focused on.

3.1 Geometry

This part focuses on the geometry generation and development part. We focused on making the geometry look as close to the real drone as possible. The essential part of this process was getting the airfoil shape from the existing drone, and the process will be described in the following section.

3.2 Obtaining the airfoil with MATLAB

In order to get the geometry closer to reality, it was essential to make the wings as accurate as possible. For this task, we used the picture from the side of the aircraft because from there, we could see the airfoil shape. After that, we used MATLAB to first generate the airfoil shape and then convert this shape into the X and Y points, which we could import easily into the OpenVSP. The process of generating the airfoil in MATLAB was fairly simple. First, we converted the original image into a grayscale image to make the edges more visible. Then we applied a Gaussian filter for accurate edge detection to recognize the airfoil shape. In the last part, we established the contours from the edge detection and set the boundary around the airfoil contour, and then the final part consisted of getting the aspect ratio from the picture and generating the 2D points.

Figure 3.1: Real wing profile captured from the side

In the figure above, we can see the picture used to generate the airfoil in MATLAB. It was difficult to even get to this picture because usually, these types of aircraft are photographed from a distance and angles where we can't really see the details.

Figure 3.2: Wing profile generated with MATLAB

In the figure above, we can see the airfoil profile as the red line and the edge as the white line. As we can see, the airfoil profile isn't the smoothest, however, because as I mentioned, we are extracting multiple 2D points, in the OpenVSP, these points represent the airfoil profile, and therefore, if we export fewer points, the profile becomes smoother in the OpenVSP than what is displayed above. The final result in OpenVSP turned out to be working with the rest of the geometry. The 2D points generated from MATLAB in practice helped to make the airfoil even smoother when imported into OpenVSP, however, I do not think that the points database was insufficient in order to keep the airfoil shape.

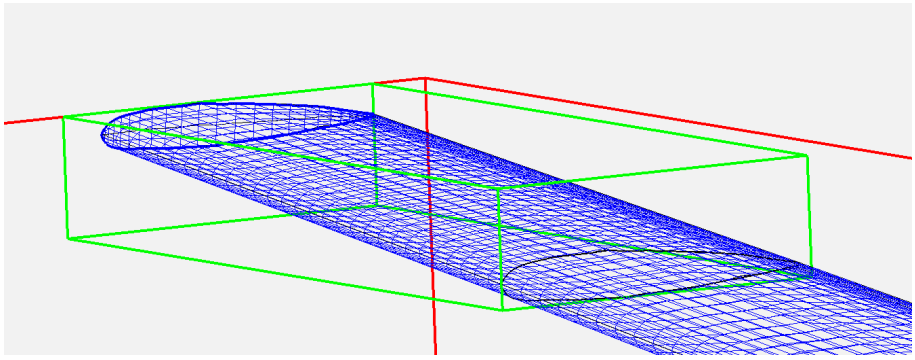

Figure 3.3: Wing geometry in OpenVSP using the generated airfoil profile

3.2.1 OpenVSP

The geometry in OpenVSP was done according to the pictures that are available with respect to the dimensions that are available. The correct airfoil profile was

obtained from MATLAB, as discussed in the previous section. The blended wing body uses an aifoil from the OpenVSP library, and the shape was done so that it resolves the real geometry as accurately as possible. On the bottom of the blended wing body is a camera or lidar; its dimensions were impossible to obtain, so it has been scaled to the body by eye. The arms that connect the tail wings to the blended wing body were also adjusted so that the overall shape matches the real one. Tail wings were assumed to use a symmetrical airfoil for stability purposes and maneuverability. Finally, the propeller used is the one from the OpenVSP library. I would like to mention that the propeller also differs from the version to version in reality; some models use 3 blade design and some use just 2 blades and of course it would be impossible to get technical parameters of it so for this purpose we will use the one from the OpenVSP library and assume that the performance will be suficient during the cruise state [3]. The drone also had an angle of attack of 5 degrees to replicate the angle of attack during the cruise.

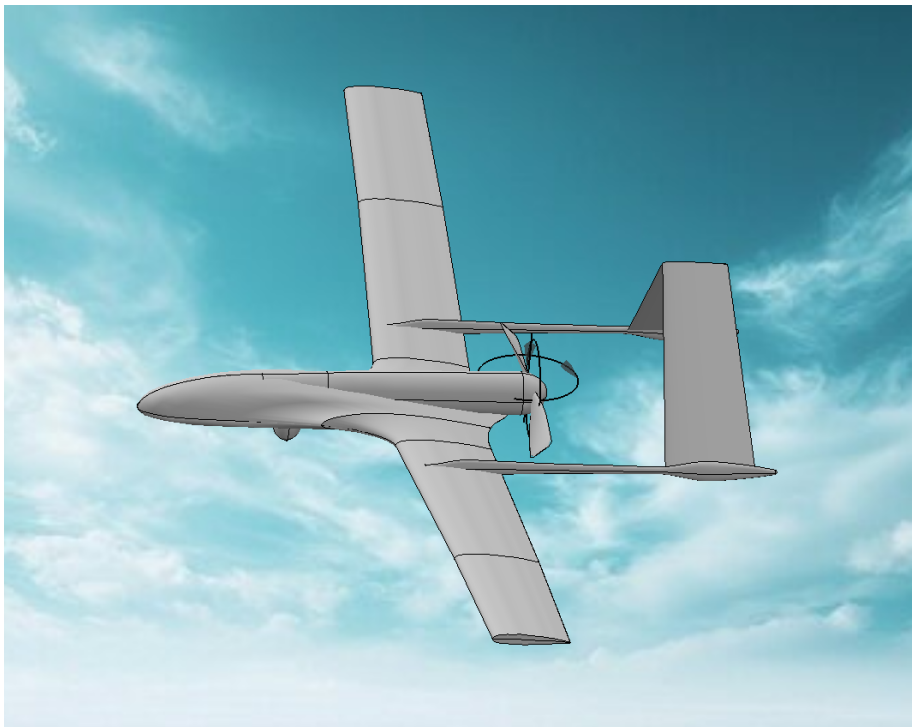

Figure 3.4: Geometry generated with OpenVSP

The dimensions that are available are very limited, but they set a boundary on the wing span, which is 12 meters, and the overall length which is around 6.5 meters but we assumed that it is with the pitot tube at the front which we dont include in this project, however it is very important for the real aircraft, but not so much in this project. The height is around 2.2 meters, but with extended landing gear, which we didn't include because we are investigating the cruise condition, that is why the height is significantly smaller [3][20].

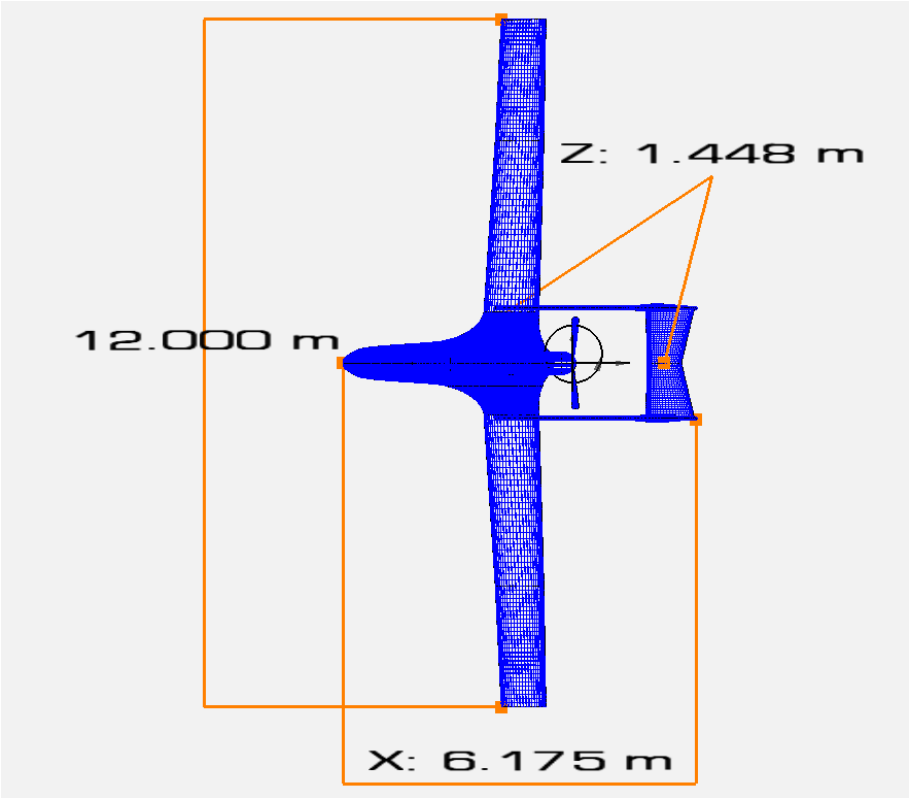

Figure 3.5: Drone dimensions according to the obtained informations

3.3 Palabos

In this section, we will describe the methodology built in order to simulate the fluid flow during the cruise conditions. For this, we used the open-source Lattice Boltzmann software called Palabos. The Palabos library is a framework for general-purpose computational fluid dynamics (CFD), with a kernel based on the LBM. It is used both as a research and an engineering tool: its programming interface is straightforward and makes it possible to set up fluid flow simulations with relative ease, or, if you are knowledgeable of the lattice Boltzmann method, to extend the library with your own models. Palabos stands for Parallel Lattice Boltzmann Solver [4][21]. The LBM solver was chosen for its speed, as in the traditional FVM, the solver needs to calculate a set of differential equations for each cell. However, in the LBM, the solver calculates just the neighbouring cells, which makes the calculations significantly faster compared to the traditional FVM. Also, the Palabos software was user-friendly and easy to use without any significant convergence issues.

3.3.1 Conversion of LBM Units

As we know, in Palabos, we are working on the mesoscopic scale, and therefore, it is essential to make sure that the LBM units are also accurate and match the Reynolds number to the real case. Because we are working in the quasi-incompressible flow, the speed of sound in the LBM is equal to the square root of 1/3, which is roughly

0.577. From the characteristic length and resolution, we can get dx and dt we set to 0.0021 [2][4]. From the Palabos, we can see that the lattice Boltzmann velocity is calculated in the form of:

$$u(LB) = inletVelocity * (\frac{dt}{dx}) \tag{3.1}$$

We know the value of the speed of sound in Lattice Boltzmann units, so to really compare the air flow velocity to the real case, we decided to make the Mach number equal to the real one during the drone cruise. This Mach number is equal to around 0.1, and to make the same in LB units, we simply multiply the velocity in LB units by the speed of sound for quasi-incompressible cases, because the velocity is low enough, we can assume no compressibility effects.

$$cs = \sqrt{1/3} = 0.577 \tag{3.2}$$

$$Ma = u(LB) * cs \tag{3.3}$$

After this, the only thing left to compare is the Reynolds number. The real case during cruise is around 8-10 million with the velocity of 70 knots according to [2] and the characteristic length of 6.175m because we simulate geometry without a pitot tube at the front, which we assumed to be 325 mm long. Because the drone during cruise reaches an altitude of around 7km, the kinematic viscosity according to the standard atmosphere, we can calculate using ρ and temperature is around 2.5-2.6e-5. From these values we can check that the Reynolds number is 8.6 million. In Palabos, we can easily put these values in the input file and get the desired Reynolds number.

3.3.2 Reynolds number

As we already mentioned, an important non-dimensional quantity to compare the fluid flow is the Reynolds number. This number is essentially the ratio of the inertial forces to the viscous forces and it is used to evaluate the flow conditions and also to compare different testing conditions or simulations, in this project we will use both the Mach number and the Reynolds number to make sure that the flow conditions are the same as during the real mission. The Reynolds number can be expressed as:

$$Re = \frac{VL}{v} \tag{3.4}$$

Here we can see that the velocity V and characteristic length L, which, as I mentioned, are considered as inertial forces, are divided by kinematic viscosity v, or the viscous forces. The Reynolds number is calculated the same way in Palabos, because we provide the inlet velocity, the characteristic length, and the kinematic viscosity [10].

3.4 Ansys static structural

For the structural analysis the Ansys static structural FEM solver was chosen in order to simulate the long-span wing deflection while providing the needed lift in

order to cruise around the desired location. From the source [3], we know that the estimated weight of the drone is around 500kg with payload; however, as an input force, we will use the average lifting force we obtain from the fluid analysis conducted in Palabos so this force might differ because of the differences from the real drone. In our case, we will assume that the lifting force is sufficient for the weight of the aircraft. This means that to achieve the most amount of efficiency, the drone needs just amount of lift so that it is sufficient for its weight. We also assume that the lifting force is mostly generated by the main wings because the tail is mostly for stability purposes and to help with maneuverability.

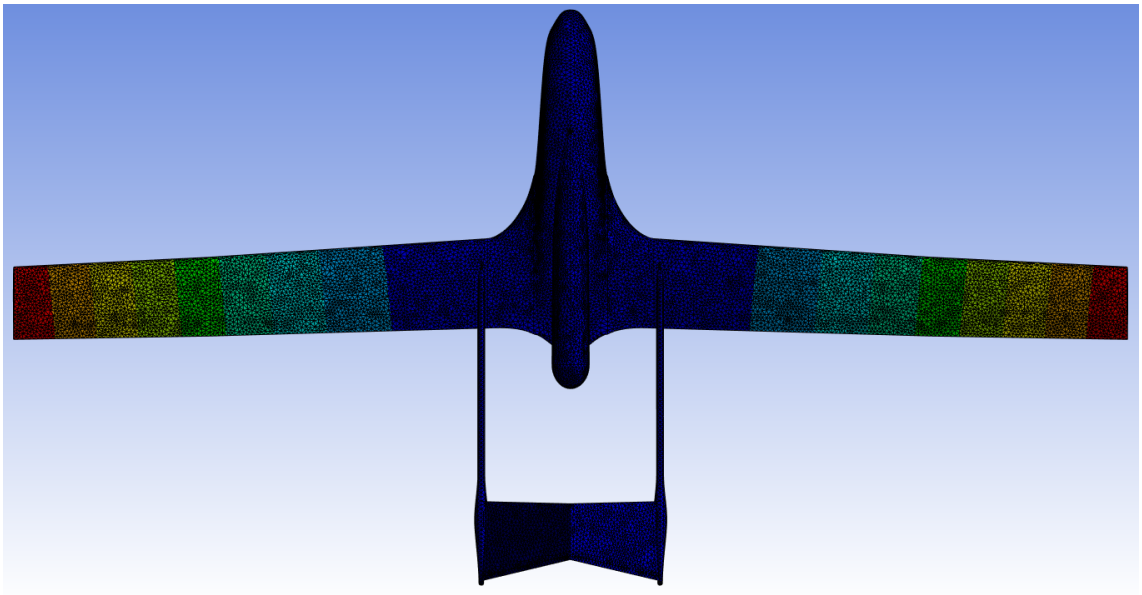

Figure 3.6: Geometry simulated in Ansys static structural solver

3.5 Ansys boundary conditions

As we already mentioned, the input force for the structural simulation will be the averaged lift force from Palabos. We simulate the deflection of the main wings, so another boundary condition that we have is the zero displacement, in every direction, of the "fuselage" or the main body of the blended wing. In reality, this main body might as well provide some amount of lift, but we consider it negligible in comparison to the wings extending from the body. In that case, we can think about the wings as built-in beams and place the force on the wings in the upward direction. Last but not least is the thrust force, which we will also have as a boundary condition to investigate its impact on the deformation.

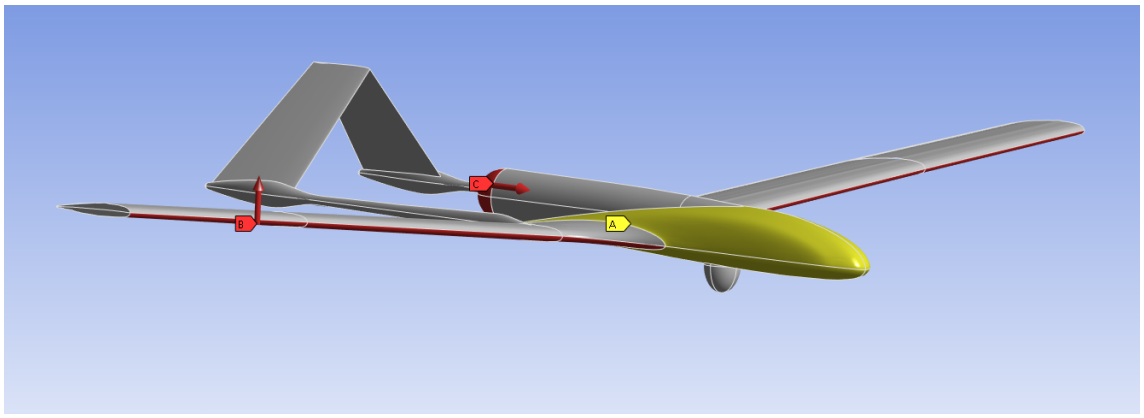

Figure 3.7: Ansys boundary conditions

In the figure above, we can see the boundary conditions set on the actual geometry where A is a displacement restraint so that portion of the aircraft doesn't move, B is the lifting force generated by the wings, and C is the thrust force of the propeller. The propeller is not included in this, as it would require its own study.

4

Results

In this section, we will discuss results obtained from the study that we performed on the long-span wing drone geometry in order to investigate both the aerodynamic and structural behavior. First, we can start by discussing the geometry that was obtained in OpenVSP, with the main wing airfoil being done with MATLAB. The dimensions and technical pieces of information were very limited for this drone; however, the geometry was made to imitate as closely as possible the existing geometry of Bayraktar TB2, for obvious reasons there are some differences, but the main dimensions like wingspan and height were known and the geometry was done maintaining these dimensions. The most important part of the geometry, which was the airfoil, we captured successfully.

4.0.1 Mesh convergence

In order to start evaluating the results from the numerical investigations, first, we have to establish a mesh that will be a reliable source of accurate results. That is why we have to evaluate the mesh, and to do that, we will conduct the mesh convergence analysis. In the figures below, we can see that in both Palabos and Ansys, the mesh converged to a certain value, and we can see that by the shape of both curves. It can be observed that they are becoming stable around one value on the Y axis, which represents the investigated parameter. These mesh convergence studies were performed before the final results were obtained, and therefore, the values of the averaged lift force and deformation do not match the final results of these investigated parameters. The mesh convergence study was done in order to make sure that the mesh quality is reliable.

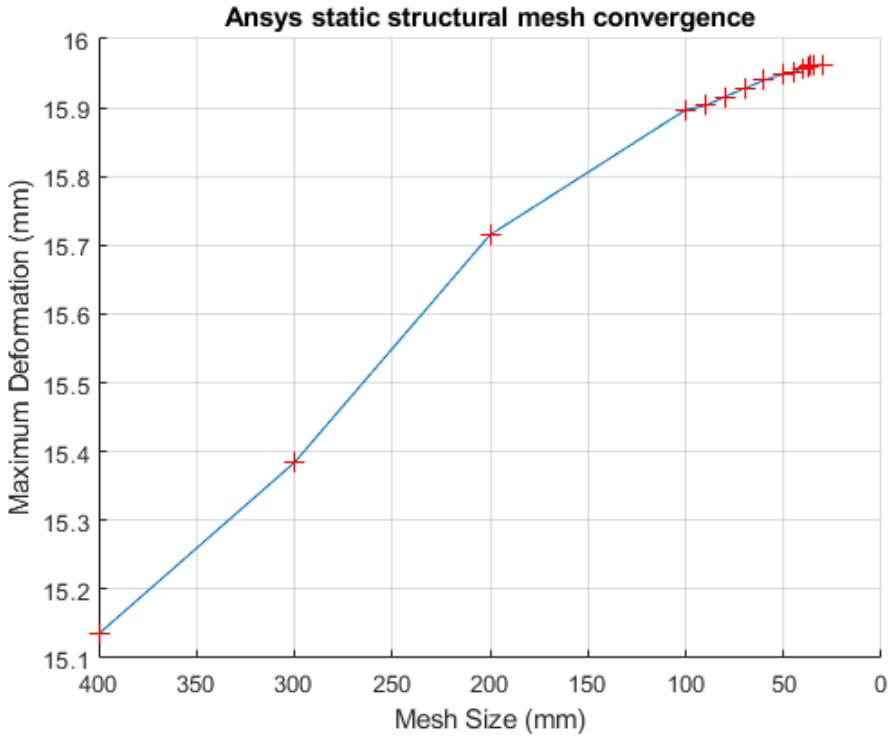

Figure 4.1: Ansys mesh convergence.

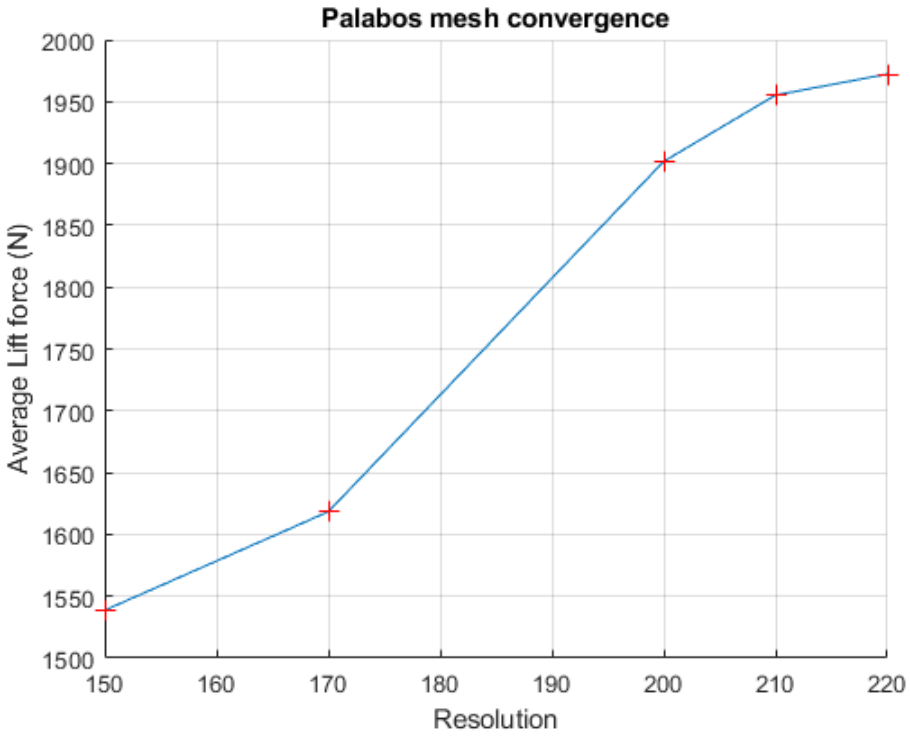

Figure 4.2: Palabos mesh convergence.

4.0.2 Palabos results

The Palabos simulation was done using one of the showCase cases named generalExternalFlow. This library was very convenient for this case, and input values, together with files, were modified to suit our case, because the geometry used in this project was significantly larger than the default sphere geometry; some adjustments were necessary in order to run the case. In this simulation, we replicated the cruise condition, which occurs at 70 knots or 130 km/h at an altitude of around 6700 meters. With this information, we know that the Mach number is around 0.1, and the Reynolds number is around 8.6 million. For the simulation to be accurate, we need to match the Reynolds number and Mach number. Another important aspect was the mesh, which we refined to the memory and computational limit, but as we saw on the mesh convergence, the mesh didn't need any more refinements as the lift and drag force were stable around the average values after the average energy stabilized.

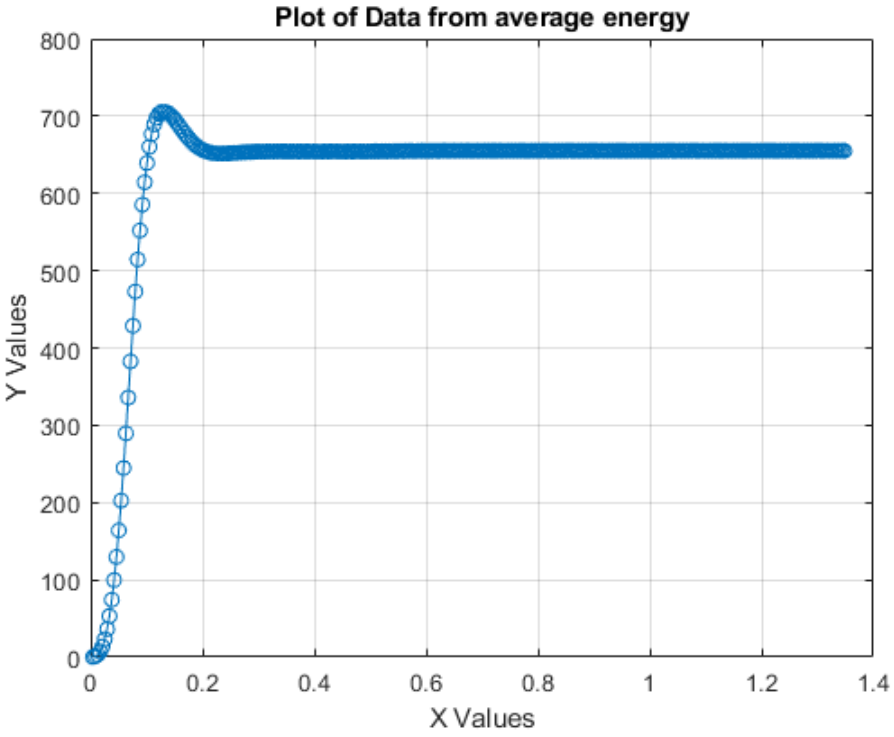

Figure 4.3: Average energy from the CFD simulation across time

On the figure above, we can see the average energy plot from the simulation, which shows the convergence of the simulation, and we can see that the simulation converges after 0.4 seconds. After this time, we can observe the important quantities such as lift and drag converge and move around the average value.

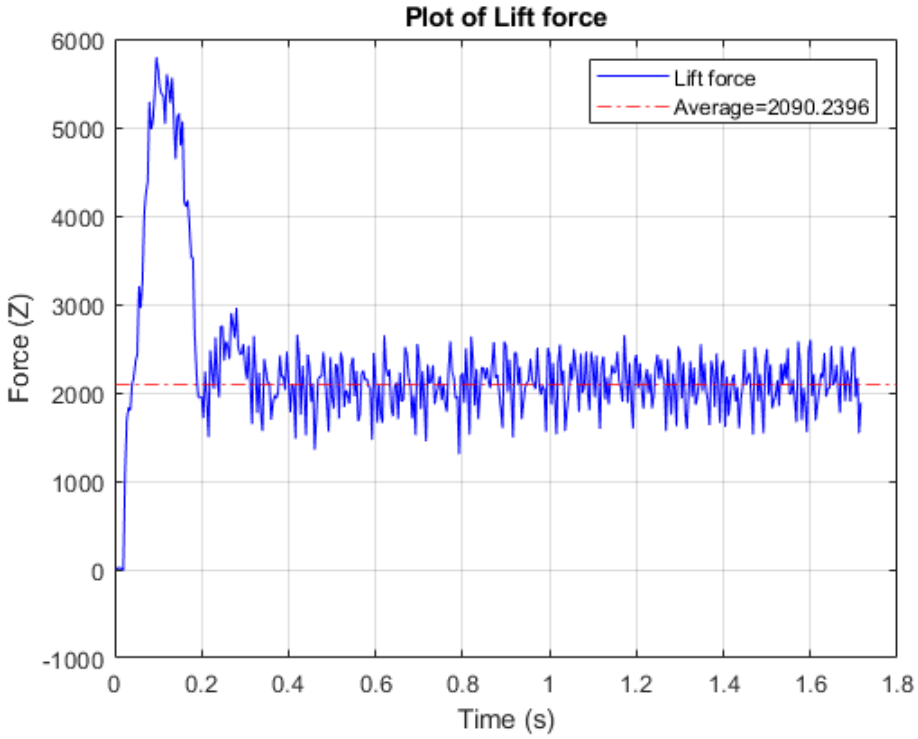

Figure 4.4: Lift force from the CFD simulation.

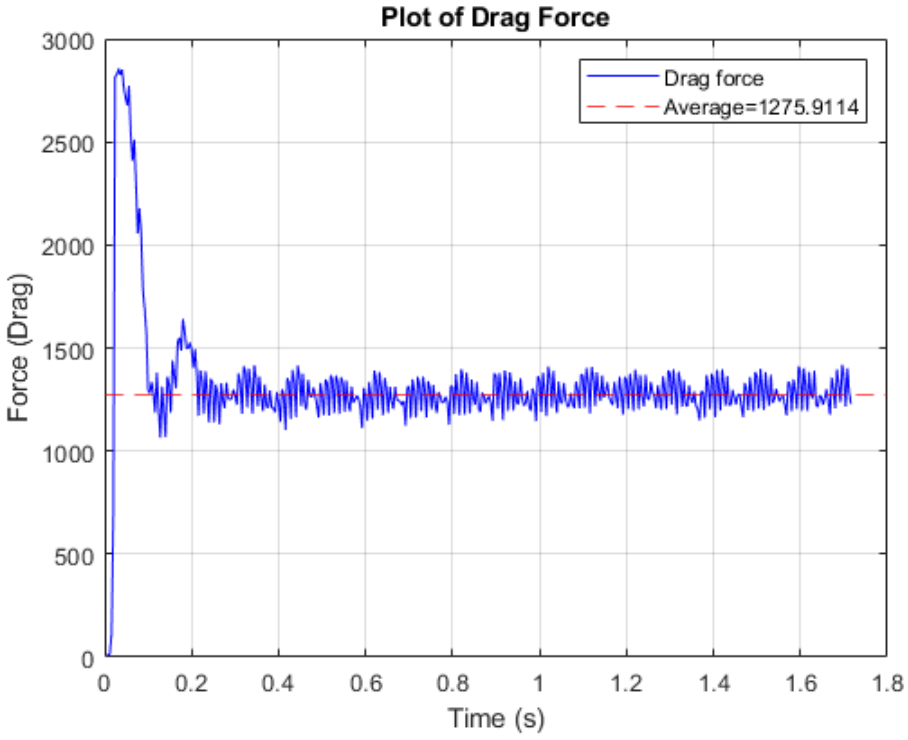

Figure 4.5: Drag force from the CFD simulation.

On the figures above, we can see the lift and drag forces from the CFD simulation. The Lift force averaged around 2090.2396 N, which is less than what was expected. Expected value for the real drone is 5000 N because of the weight, which is 500 kg, but this offset can be explained by the already mentioned differences in geometries and also performance estimations. The drag force averaged around 1275.9114 N. The angle of attack that produced the most lift was around 6 degrees, and the flow velocity was around Mach 0.1.

4.0.3 Ansys results

In the Ansys, we established a structural simulation to investigate the structural deformation of the wings. The Lift force from the CFD simulation was boundary condition on the wings with the displacement restraint on the main body and also the thrust force which was considered equal to the drag.

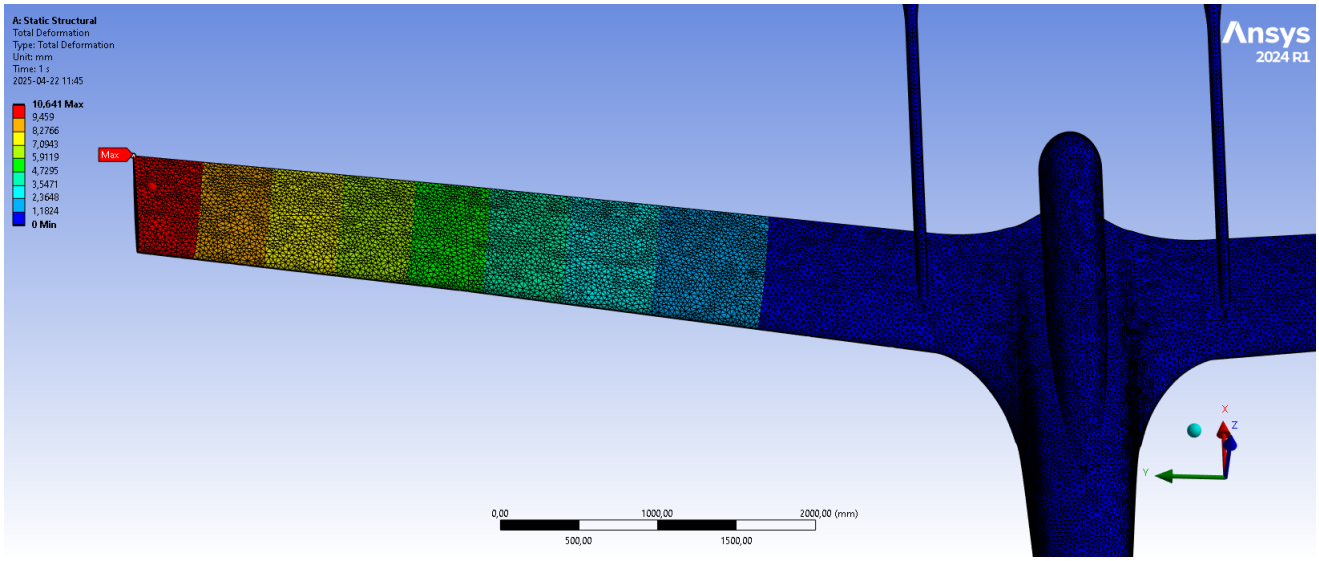

Figure 4.6: Ansys static structural simulation result of the deformation magnitude

In the figure above, we can see the results from the structural solver, and we can see that the maximum deformation is located at the tip of the wing at the trailing edge. We can also see the value of the maximum deformation, which has a magnitude of 10.641 mm. We can also see that the thrust force has no impact on the results, as this force is significantly smaller than the lift force.

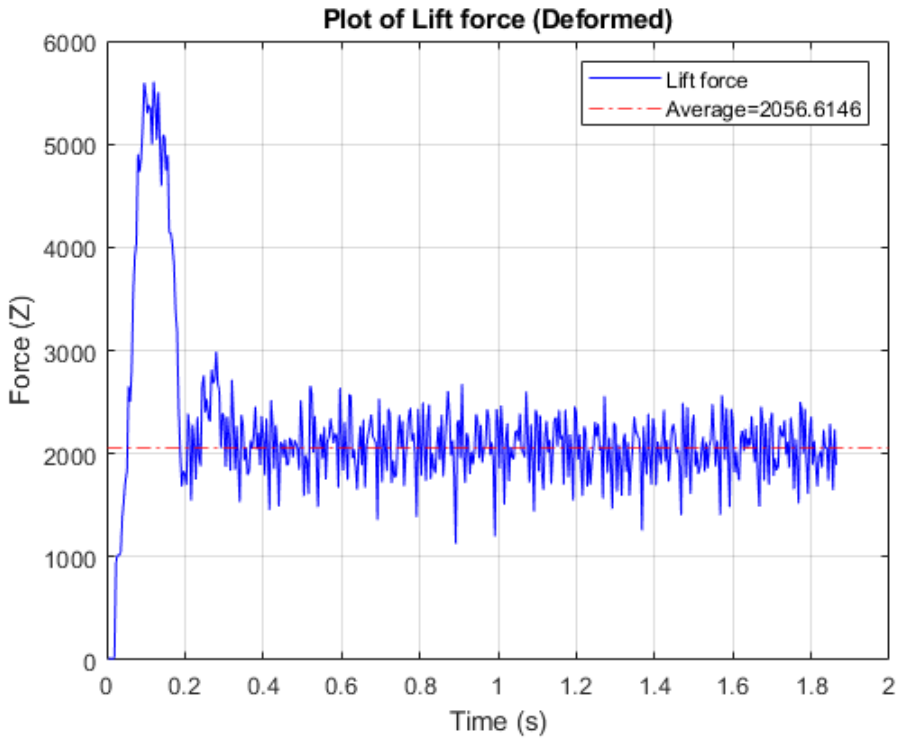

Figure 4.7: Lift force from the CFD simulation of the deformed geometry.

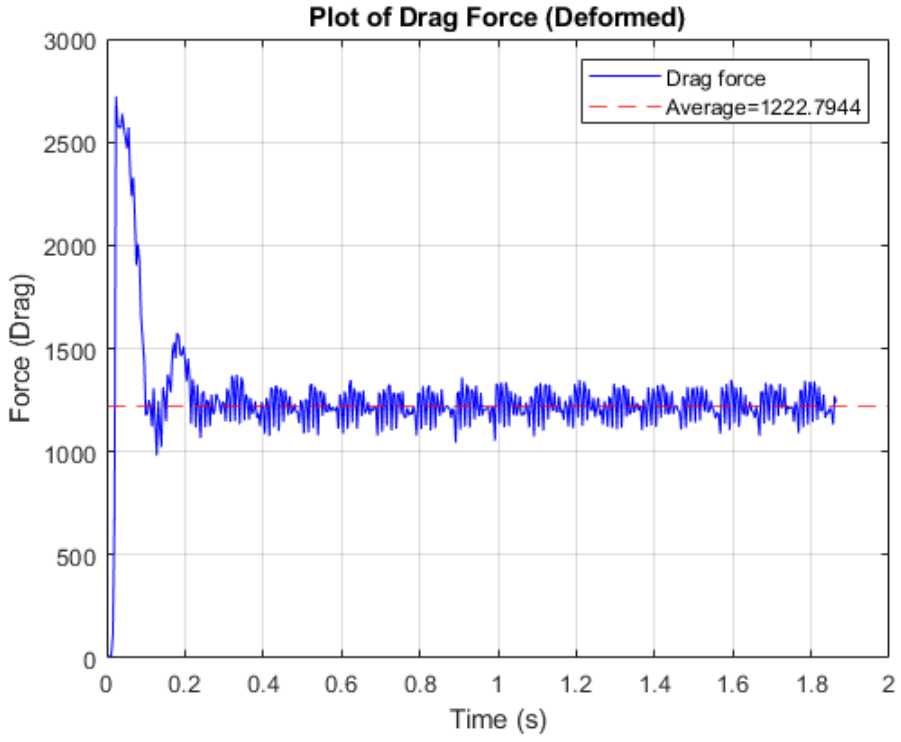

Figure 4.8: Drag force from the CFD simulation of the deformed geometry.

As we can see from the figures above, the Lift force and the drag force after the deformation have changed by the magnitude of 33.625 N in lift and 53.117 N in drag, both of these forces have decreased. It can be argued that this slight decrease can also be the result of the deviation, because this change is of a relatively small magnitude, and the calculated standard deviation was 280.2621 N or 13.41 %, and this slight change is in the range of this standard deviation. However even if the there was a this slight change, we think that the performance change can be neglected, and that there would be need for the investigation in the off-design condition when the lift force is significantly higher for example during take off or climb condition, when the AOA of the drone is increased significantly.

5
Conclusion

The objective of this project was to study the fluid-structure interaction (FSI) on the long-span wing drone geometry and assess its effect on aerodynamic performance, and investigate the deformation of the wing. To achieve this, we conducted numerical investigations using Computational Fluid Dynamics (CFD) and Finite Element Method (FEM). At the beginning, we developed the CFD simulation to determine the aerodynamic forces acting on the long-span wing drone geometry. From this simulation, we got the lift force with a magnitude of 2090.2396 N, and 1275.9114 N of drag force. In the next step, we established the FEM simulation to analyze the deformation and stresses resulting from these aerodynamic loads and to investigate the deformation resulting from these forces. The deformation resulting from this simulation had a magnitude of 10.641 mm, which was the maximum deformation located at the tip of the wing at the trailing edge. The final step involved coupling these two software tools, in which we simulated the deformed geometry from the structural simulation to investigate the change in aerodynamic performance. The CFD analysis of the deformed geometry obtained from the structural analysis provided us with approximately 2056.6146 Newtons of lifting force at cruise velocity and 1222.7944 Newtons of drag force, which was equal to 70 knots or 130 km/h. This change can be considered negligible because we found that it was within the range of the standard deviation. We can argue that this deformation does not affect the lift or the overall performance significantly, however this study was performed during cruise conditions, which means that the forces and structure are coherently co-operating, however as this is design case, further study in the off-design case would be very valuable in order to investigate the deformation and aerodynamic performance changes when the lift force significantly increases and the aircraft becomes more prone to stall, for example during take off, or climb conditions. If a significant change in performance is observed, further studies in the sandwich structure would be needed to increase the stiffness and reduce the deformation.

6
Future work

This topic has an unlimited amount of work that can be done, in my opinion, but I would like to mention some interesting topics that I would pay attention to. First things first, the geometry itself is topic on its own and as we know, the wings aren't just extruded airfoils in reality, they are made out of ribs and spars which was not in scope of my work but it would be really interesting to see the behavior of the more detailed wing geometry. Another field of future work could be the off-design conditions. In this project, I was focused on the cruise condition, which is also the design condition, but it would be really interesting to see the performance variation for example during climb or take-off conditions, because in these two scenarios the lift significantly increases, which means that the stress on the wings will be also higher and therefore the deformation will most likely increase as well. These are just a few things that I find interesting to investigate, but as I said, the work that can be done is unlimited, and I think everyone can find their own.

Bibliography

[1] https://www.grc.nasa.gov/www/k-12/VirtualAero/BottleRocket/airplane/forces.html

[2] Timm Krüger, Halim Kusumaatmaja, Alexandr Kuzmin, Orest Shardt, Goncalo Silva, Erlend Magnus Viggen, "The Lattice Boltzmann Method Principles and Practice", 2017.

[3] Léo PÉRIA-PEIGNÉ, "TB2 Bayraktar Big Strategy for a Little Drone", 2023.

[4] Palabos User Guide Release 1.0 r1, 2019.

[5] RAMMOHAN SUBRAMANIA RAJA, Coupled fluid structure interaction analysis on a cylinder exposed to ocean wave loading, 2012.

[6] Yue Liu, Bernd Zwingmann. Carbon Fiber Reinforced Polymer for Cable Structures—A Review (2015). Researchgate.net. Published.

[7] Adam Kašička, "Meranie zaťaženia spojovacej tyče na zavesení prednej nápravy vozidla", Bachelor thesis, Slovak University of Technology in Bratislava, 2023.

[8] https://en.wikipedia.org/wiki/Hooke%27s_law, 2017.

[9] https://ultmeche.com/strain-formula/

[10] Doug McLean, "UNDERSTANDING AERODYNAMICS ARGUING FROM THE REAL PHYSICS", 2013.

[11] George Papadakis, C. G. Giannopapa, "LINEAR STABILITY ANALYSIS AND APPLICATION OF A NEW SOLUTION METHOD OF THE ELASTODYNAMIC EQUATIONS SUITABLE FOR A UNIFIED FLUID-STRUCTURE-INTERACTION APPROACH, 2008.

[12] Z.Yun, Y.Hui, “Coupled fluid structure flutter analysis of a transonic fan” Chinese Journal of Aeronautics, vol.24, 2011, 258-264.

[13] Lucintel Brief , “Growth Opportunity in Global UAV Market”, 2011.

[14] Yu-shan Meng, Li Yan, Wei Huang , “Structural design and analysis of a composite wing with high aspect ratio”, 2019.

[15] Mikel Ezkurra, Jon Ander Esnaola, Manex Martinez Agirre, Unai Etxeberria , “Analysis of One-Way and Two-Way FSI Approaches to Characterise the Flow Regime and the Mechanical Behaviour during Closing Manoeuvring Operation of a Butterfly Valve”, 2018.

[16] AdamKasicka, Bilal Mohammed Sajjad Siddiqui, Maulik Rakesh Rajput, “Fluid-Structure Interaction Analysis On The Rear Wing Of A Formula Student Car”, 2025.

[17] Christine Unger, “BENDING INSTEAD OF SNAPPING”, 2020.

[18] Yue Liu, Bernd Zwingmann, “Carbon Fiber Reinforced Polymer for Cable Structures—A Review”, 2015.

[19] M. R. A. Hutagalung, A. A. Latif, H.A. Israr, “STRUCTURAL DESIGN OF UAVSEMI-MONOQUE COMPOSITE WING”, 2016.

[20] `https://www.testo.com/en-US/straight-pitot-tube-500-mm/p/0635-2143`, 2025.

[21] `https://palabos.unige.ch/`

A

MATLAB Code for Airfoil Extraction

Listing A.1: MATLAB script for airfoil shape extraction

```
imagePath = 'airfoil3.png';
img = imread(imagePath);

grayImg = rgb2gray(img);
figure;
imshow(grayImg);
title('Gray');
edges = edge(grayImg, 'canny');

smoothImg = imgaussfilt(grayImg, 2);
edges = edge(smoothImg, 'canny');

se = strel('disk', 5);
closedEdges = imclose(edges, se);

figure;
imshow(closedEdges);
title('Closed Edges');

[B, L] = bwboundaries(closedEdges, 'noholes');

figure;
imshow(closedEdges);
hold on;
for k = 1:length(B)
    plot(B{k}(:,2), B{k}(:,1), 'b', 'LineWidth', 1);
end
title('All Detected Boundaries');

imageWidth = size(img, 2);
imageHeight = size(img, 1);
aspectRatio = imageWidth / imageHeight;
```

```
figure;
imshow(closedEdges);
hold on;

boundarySizes = cellfun(@length, B);
[~, idx] = max(boundarySizes);

boundary = B{idx};
plot(boundary(:,2), boundary(:,1), 'r', 'LineWidth', 1.5);
title('Airfoil Contour');

x = boundary(:,2);
y = boundary(:,1);
xNorm = (x - min(x)) / (max(x) - min(x));
yNorm = (y - min(y)) / (max(y) - min(y));
```

B

Geometry Parameters

Table B.1: Drone geometry and flight parameters

Parameter	**Value**	**Unit**
Wingspan	12.0	m
Fuselage Length	∼6.175	m
Cruise Velocity	130	km/h
Altitude	6700	m
Reynolds Number	8.6×10^6	–
Mach Number	0.1	–
Airfoil Source	Extracted from image	–

C

Ansys Simulation Boundary Conditions

- **Lift Force (Y-axis)**: 2282 N applied to main wing surfaces
- **Fixed Support**: Fuselage constrained in all degrees of freedom
- **Drag Force (X-axis)**: Applied as reaction force equal to estimated drag
- **Material**: Carbon Fiber Composite (from Ansys library)

D

Palabos Simulation Configuration

Table D.1: Palabos input parameters and derived quantities

Input Parameter	**Value**
Lattice resolution (dx)	0.0021
Inlet velocity (u)	0.125 (LB units)
Kinematic viscosity (ν)	2.56×10^{-5}
Characteristic length (L)	6.175 m
Speed of sound (c_s)	$\sqrt{1/3} \approx 0.577$
Mach number (Ma)	$u \cdot c_s = 0.1$
Reynolds number (Re)	8.6 million

DEPARTMENT OF MECHANICS AND MARITIME SCIENCES
CHALMERS UNIVERSITY OF TECHNOLOGY
Gothenburg, Sweden
www.chalmers.se

CHALMERS
UNIVERSITY OF TECHNOLOGY